NANO LETTERS

2008
Vol. 8, No. 3
935-940

Short Range Plasmon Resonators Probed by Photoemission Electron Microscopy

Ludovic Douillard,* Fabrice Charra, and Zbigniew Korczak†

Commissariat à l'Energie Atomique Saclay Direction des Sciences de la Matière - Institut Rayonnement Matière de Saclay - Service de Physique et Chimie des Surfaces et Interfaces, F-91191 Gif sur Yvette, France

Renaud Bachelot, Sergei Kostcheev, Gilles Lerondel, Pierre-Michel Adam, and Pascal Royer

Laboratoire de Nanotechnologie et d'Instrumentation Optique, ICD CNRS FRE 2848, Université de Technologie de Troyes, 12 rue Marie-Curie, BP 2060,

F-10010 Troyes, France

Received January 8, 2008; Revised Manuscript Received January 29, 2008

ABSTRACT

Short range surface plasmon resonators are investigated at the nanometer scale. Gold nanorods (30 nm in diameter) were microfabricated and probed by photoemission electron microscopy under direct laser light excitation. Resonances presenting various numbers of lobes occur for specific rod lengths. A simple analytical model shows that the successive resonant lengths differ by a multiple of one-half of the wavelength of the supported short-range surface plasmon polariton.

The integration of optics into ever smaller devices is hampered by the long standing barrier of the diffraction limit, namely, the impossibility to confine light below its natural wavelength, i.e., λ_0 in free space or λ_0/n in a material of refractive index n. In parallel, solid state physics, making use of electrons, allows for high integration densities at the expense of low-band-pass devices. Surface plasmon polaritons (SPPs) are electromagnetic surface waves coupled to free electrons at metal dielectric interfaces. As electromagnetic waves, they share the same high working frequency as light; using free electrons as supporting particles they allow for spatial confinements over distances smaller than the wavelength of light. So surface plasmon polariton waves offer a unique opportunity for scaling down photonic devices to the nanometer range.[1]

Among the most traditional electromagnetic devices, antennas,[2–4] by converting free-space electromagnetic radiation into localized ones, would be especially interesting to be scaled to nanometer dimensions and optical frequencies. In the radio frequency regime, simple antennas consist in metal resonators, such as rods whose lengths L are in simple relation to the incoming or outcoming free radiation wavelength λ_0. As the frequency approaches optical regime, and the rod diameter approaches the material skin depth, SPP dispersion relation departs from the line of light. Indeed interactions between SPPs propagating along the rod walls give rise to coupled modes, known as short-range surface plasmon polaritons (SR-SPPs).[5,6] The resonance frequencies are then dictated by the significantly shorter SR-SPP wavelength $\lambda_{SR\text{-}SPP}$, whose value depends on the geometry and material properties.[5–10] This further confines the optical fields around the rod but also introduces severe phase-matching conditions for the resonant mode excitation by free space waves with natural wavelength $\lambda_0 > \lambda_{SR\text{-}SPP}$.

In this article, we investigate short-range surface plasmon polariton resonators at the nanometer scale by photoemission electron microscopy (PEEM).[11–16] In particular, we directly observed coupled plasmonic modes on Au nanorods 30 nm in diameter. By adapting antenna theory, a simple analytical model is derived, enabling the interpretation of rod resonances at optical frequencies. Compared to recent studies by optical microscopy,[7,17–19] scanning near field microscopy (SNOM)[20,21] and photoemission electron microscopy[15] dealing with noninteracting SPPs excited in

* Corresponding author. E-mail: ludovic.douillard@cea.fr.
† Permanent address Institute of Physics and Nanotechnology Center, Maria Curie-Skłodowska University, Pl. M. Curie-Skłodowskiej 1, P-20031 Lublin, Poland.

10.1021/nl080053v CCC: $40.75
Published on Web 02/21/2008

(sub)micrometer objects, the present work addresses the coupled nature of the plasmonic waves inherited from the drastic reduction of object sizes. While SR-SPPs are called to play an important role into the ever smaller photonic devices, the plasmonics of metal objects of characteristic sections below the evanescent field decay length is largely unexplored.

Single Au nanorods of length L have been microfabricated by electron-beam lithography. The rod lengths sample the interval (50−925 nm) in steps of 25 nm. The rod cross section is rectangular, 35 nm in height and 30 nm in width. Objects are distributed according to a 6 × 6 matrix and are 10 μm distance apart. The whole array size is a square of 80 μm length in side. In parallel long rods of length L up to 4 μm have been prepared. Size and shape of individual objects deviate from their expected values by less than 10% as estimated from scanning electron microscopy (SEM). The substrate consists of a 95 nm thick indium tin oxide (ITO) coated silica glass.

The excitation light source used for PEEM measurements is a continuous wave (CW) mode-locked Ti:sapphire laser system (Tsunami, Spectra Physics Inc.) delivering IR photons in the 740–880 nm range (1.675−1.41 eV). The pulse repetition rate is fixed at 80 MHz. Each pulse exhibits a profile of 80 fs duration. Two different angles of beam incidence are used, namely, $\alpha = 0°$ and 75° (90° and 15° with respect to the surface plane). At normal incidence ($\alpha = 0°$) the light is focused onto the sample through a 500 mm focal length lens yielding a circular spot of 730 μm in diameter. At grazing incidence ($\alpha = 75°$), a 200 mm focal length lens is used and the spot is an elongated ellipse whose minor and major axes amount to 260 μm × 1160 μm. The peak power densities delivered at the sample surface are in the range 50−150 MW/cm^2. The p-polarization state is selected by a half-wave plate.

The photoemission electron microscope used is a commercial instrument (Elmitec GmbH LEEM\PEEM III) operating in ultrahigh vacuum at pressure in the low range of 10^{-10} mbar. Lateral spatial resolutions of 10 and 25 nm are routinely achieved in low-energy electron diffraction (LEEM) and photoelectron emission (PEEM) imaging modes, respectively.[22] The instrument operates in total electron yield (no energy filtering).[23] The real-space images are recorded via a charge-coupled device (CCD) camera and digitized for further analysis (Argus 20, Hamamatsu Inc.). In PEEM imaging mode, the measured brightness in a given image area is proportional to the electron emission from that area. Integrated PEEM signal is computed in two steps: (i) background subtraction, i.e., removing of a regression plane, (ii) integration of the pixel values over a representative image area. The work function of amorphous Au is in the 4.6−5.1 eV range, and no direct one photoemission is expected. We measured that the PEEM signal is proportional to the cubed incident intensity, so the electron emission has its origin in a three-photon absorption process. The collected electron emission reflects the optical near field at the surface of metallic nanoobjects. Compared to optical microscopy,[7,17–19] scanning field optical microscopy (SNOM)[20,21,24], and electron excitation based techniques,[25,26] the photoemission electron microscopy permits nanoscale analysis of single metal objects under direct laser light illumination. More details about the PEEM experiment can be found in ref 14.

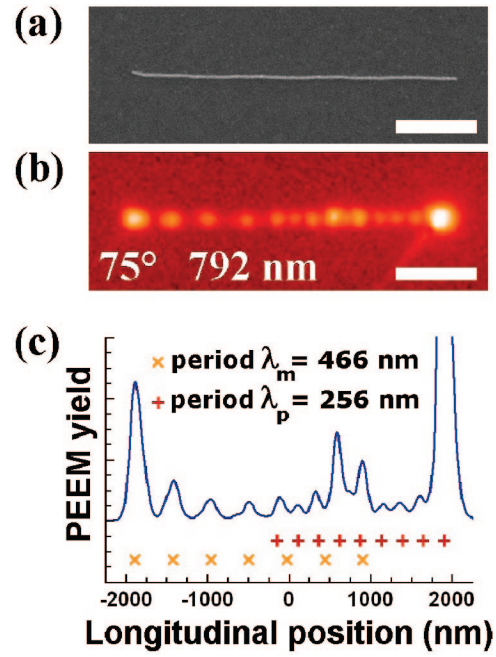

Figure 1. Off-resonant single Au nanowire investigation. (a) SEM picture of a 4 μm long nanowire. (b) PEEM near field mapping (grazing incidence $\alpha = 75°$, p polarization, excitation wavelength $\lambda_0 = 792$ nm, incident power $P = 110$ MW/cm^2). Longitudinal resolution is 41 nm;[19] color scale is logarithmic. (c) Profile of the photoemission yield. Scale bar on both images is 1 μm.

The realization of plasmon-based resonators working in the optical frequency regime is based on the guiding capabilities of metal nanowire of subwavelength cross sections.[21] For sectional radii R comparable with the skin depth of the metal, the rod walls support coupled plasmon polariton modes. As previously discussed, the coupled mode we are interested in corresponds to the short-range SPP waves.[5,6] Being efficiently reflected at rod ends, SR-SPP waves are likely to give birth to strong resonance effects for specific rod lengths. In addition, SR-SPP waves allow for strong field confinement at the expense of important propagation losses, a latter aspect directly exploited by the photoemission electron microscopy for object imaging. Quantitatively, at 800 nm excitation wavelength, a SPP propagating along a single Au/vacuum interface possesses an evanescent field decay length of 25 nm on the metal side. The sectional radii of the microfabricated nanorods are in the range 30−35 nm and so fulfill the dimensional requirement for strong coupling leading to SR-SPP excitation.

A particularly simple geometry of a plasmon waveguide is a long thin metal rod. We start the study with single 4 μm long nanowires. Figure 1a displays the picture of one typical microfabricated object as seen by SEM. Figure 1b shows the associated PEEM image acquired under IR light excitation (p polarization, grazing incidence along main rod axis, excitation wavelength $\lambda_0 = 792$ nm), and Figure 1c shows the corresponding profile of the photoemission yield along the

wire axis. The propagation of the plasma waves along the nanowire is readily evidenced through the establishment of standing-wave patterns at both edges. The PEEM signal oscillates with a period $\lambda_m = 466$ nm at the leading edge while the measured period at the opposite right edge is shorter and amounts to $\lambda_p = 256$ nm. The peaks in the 500–1000 nm region of the photoemission profile present an unexpectedly high intensity. This phenomenon, not affecting peak positions, is tentatively attributed to topographic peculiarities.

The observed interference pattern can be rationalized by considering the propagation of longitudinal electron charge oscillations along a one-dimensional conductor under full field excitation. The 1D Helmholtz wave equation with excitation and damping terms is

$$\partial_t^2 F = V_\varphi^2 \partial_x^2 F + \frac{1}{\tau}\partial_t F + \frac{qE_0}{m_q} e^{i(\omega t - k_{||}x)} \quad (1)$$

where F represents the amplitude of the charge displacement from equilibrium along the wire axis x, V_φ the phase velocity of the longitudinal coupled plasma wave, τ its lifetime, and $E_0 e^{i(\omega t - k_{||}x)}$ the distributed CW exciting field acting on charge q of mass m_q. F has the dimension of a length and accounts for the amplitude of the surface plasma oscillations. These coherent charge fluctuations are accompanied by a mixed transversal and longitudinal electromagnetic field. The stationary solutions of eq 1 have the general form

$$F(x,t) = \left(A_p e^{+iKx} + A_m e^{-iKx} - \frac{qE_0/m_q}{V_\varphi^2(K^2 - k_{||}^2)} e^{-ik_{||}x}\right) e^{i\omega t} \quad (2)$$

with $K = ((\omega^2 - i\omega/\tau)/V_\varphi^2)^{1/2}$. They consist of two counterpropagating plasmonic free waves with complex wavevectors $\pm K$ ($K = K_1 + iK_2$ with K_1 and K_2 real), superimposed to a forced wave with the same wave vector $k_{||}$ as the excitation in the rod direction. K_2 translates into a damping length of the SR-SPP intensity $L_{SR\text{-}SPP} = 2\pi/2K_2$. Because of the finite size of the rod, the first two free-wave terms in eq 2 only exist at system boundaries, whereas the force-wave term remains present and unchanged for an infinite rod. At the leading edge, free and forced waves propagate in the same direction yielding a long standing wave period λ_m verifying $\Delta K_m = K_1 - k_{||} = 2\pi/\lambda_m$; at the opposite edge, counterpropagation results in a shorter period λ_p with $\Delta K_p = K_1 + k_{||} = 2\pi/\lambda_p$.[16,27]

Both beating periods (λ_m, λ_p) can be identified experimentally which allows estimation of the SR-SPP natural wavelength $\lambda_{SR\text{-}SPP} = 2\pi/K_1$ using either λ_m or λ_p. One obtains $\lambda_{SR\text{-}SPP} \approx 300 \pm 25$ and 370 ± 35 nm, respectively. Beyond measurement uncertainties, the actual spread between the two $\lambda_{SR\text{-}SPP}$ values obtained using either λ_m or λ_p is mainly attributed to unintentional rod radius differences between the two nanowire ends (for microfabricated rods $\Delta R/R \sim 10\%$). The average value $\lambda_{SR\text{-}SPP} = 335$ nm is significantly shorter than the free-space excitation wavelength $\lambda_0 = 792$ nm. This demonstrates the guided-wave nature of the rod SR-SPP waves. In addition, the SR-SPP attenuation lengths can be obtained by direct fitting of the measured near field decay profile along the propagation direction, yielding $L_{SR\text{-}SPP} \approx 3300 \pm 500$ nm (Figure 1c).

Adopting an approximation proposed in ref 28 for the dispersion relation of the SR-SPP for an infinite cylinder of sectional radius R

$$\lambda_{SR\text{-}SPP} = 2\pi R\left(a_1 + a_2 \frac{\lambda_0}{\lambda_0^p}\right) \quad (3)$$

where λ_0^p is the free-space wavelength at plasma frequency of the metal assumed to obey a Drude model: dielectric constant $\epsilon(\lambda_0) = \epsilon_\infty - (\lambda_0/\lambda_0^p)^2$. For Au, we take $\epsilon_\infty = 11$ and $\lambda_0^p = 138$ nm. The (a_1, a_2) coefficients are numerically computed from the relations given by[28,29] using an effective dielectric constant ϵ_s corresponding to the weighed average, over a rectangular cross section, of the dielectric constants of vacuum $\epsilon_{Vac} = 1.0$ and ITO substrate ϵ_{ITO} (800 nm) = 3.69, i.e. $\epsilon_s = (3\epsilon_{Vac} + \epsilon_{ITO})/4 = 1.67$. This yields $\lambda_{SR\text{-}SPP} \approx 331$ nm for $R = 19.5 \pm 2$ nm, in agreement with the above experimental estimation. For comparison the wavelength of the corresponding SPP waves propagating along a single Au/vacuum plane interface is 774 nm,[30] shedding light on the strong SPP coupling. The observed damping constant is also consistent with a rough estimate of the SR-SPP damping length as estimated from the product of the group velocity[31] $V_G = (2\pi/(\lambda_0^p)R(\ln(\lambda_{SR\text{-}SPP}/2(\pi R))^{1/2}c \approx 0.885c$ and the typical plasmon lifetime[32] of a nanoparticle $\tau_{SPP} \sim 5-10$ fs, which gives $L_{SR\text{-}SPP} \approx 1328-2655$ nm. Similarly, direct comparison to the damping length calculated for a free SPP propagating on a Au perfect surface,[30] i.e., 44.5 μm at 800 nm excitation wavelength, demonstrates the short ranging character of the surface plasmon polaritons inherited from the reduction of object size.

Beyond the above considerations, the choice of appropriate bordering conditions allows one to be more precise with the detailed SR-SPP field distribution. By imposing the charge motion to be zero at both rod end facets, one obtains the exact solution for a propagation length extending from $x = -L/2$ to $x = +L/2$

$$F(x,t) = \frac{qE_0/m_q}{V_\varphi^2(K^2 - k_{||}^2)}\left(\frac{\cos(k_{||}L/2)}{\cos(KL/2)}\cos(Kx) + i\frac{\sin(k_{||}L/2)}{\sin(KL/2)}\sin(-Kx) - e^{-ik_{||}x}\right) e^{i\omega t} \quad (4)$$

As previously pointed out, for long rods, eq 4 corresponds to two counterpropagating surface plasmon waves with maximum amplitude at a rod boundary and decaying toward the rod center. Yet, for rod lengths of the order or below $L_{SR\text{-}SPP}$, these two waves can interfere together, as accounted for in eq 4 through the $\cos(Kx)$ and $\sin(Kx)$ terms. This yields Fabry–Perot-like resonances for $K_1 L = m\pi$, with m an integer mode index, characterized in that the free-wave terms in eq 4 become preponderant over the forced-wave term through either the $\cos(KL/2)$ or the $\sin(KL/2)$ denominators (odd-m or even-m modes, respectively). To refined phase retardation at end reflection, correction can be introduced by taking $L + 2R$ as the actual propagation length.[28] The resonant vacuum wavelength of the mode m can then be derived by combining eqs 3 and 4 as

$$\lambda_0^{Res}(m) = \frac{\lambda_0^p}{a_2}\left(\frac{1}{m\pi}\frac{L+2R}{R} - a_1\right) \quad (5)$$

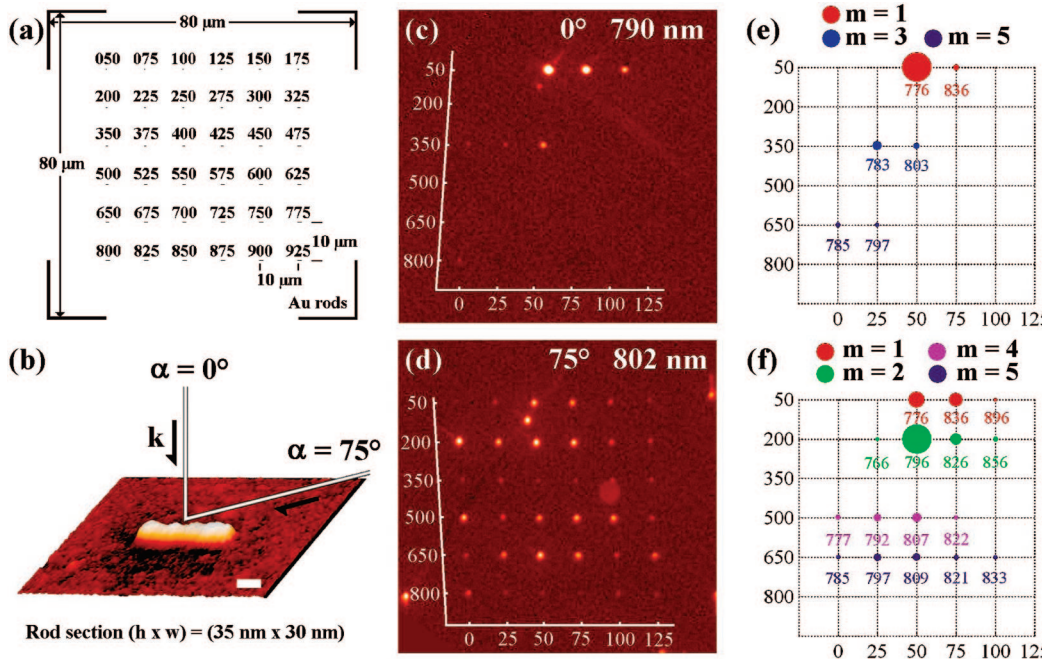

Figure 2. Systematic Au nanorod array investigation. (a) Geometry of the microfabricated sample. The L (nm) rods are organized according to a 6 × 6 matrix grid, 80 μm in side. Objects are 10 μm apart. The rod length samples the interval (50−925 nm) in steps of 25 nm. (b) SEM picture of the L = 375 nm Au nanorod. Scale bar is 100 nm. (c) PEEM imaging of the 6 × 6 resonator grid under IR laser light illumination. Field of view 80 μm, incidence angle $\alpha = 0°$, excitation wavelength $\lambda_0 = 790$ nm, incident power $P = 40$ MW/cm^2, longitudinal excitation field. Color scale is logarithmic. (d) Same as (c) but with incidence angle $\alpha = 75°$, $\lambda_0 = 802$ nm, $P = 70$ MW/cm^2, p polarization. Note that the PEEM signal-to-noise ratio is increased in (d) compared to (c). (e, f) Computed spectral responses of the SR-SPP resonator grid. For each rod length L, the displayed number is the predicted resonance wavelength λ_0^{Res} (m), the spot area is proportional to the resonance intensity with $L_{SR\text{-}SPP} = 3300$ nm and taking into account a three-photon absorption process (logarithmic scale), the spot color indicates the m-resonance order. Rod radius is $R = 16.5$ nm. (e) Normal incidence $\alpha = 0°$. (f) Grazing incidence $\alpha = 75°$.

We now move on to the systematic experimental investigation of short-range surface plasmon polariton resonators at the nanometre scale by photoemission electron microscopy. Figure 2a shows the geometry of the microfabricated resonator array made by electron beam lithography. It consists of a 6 × 6 grid, whose rod elements sample the length interval (50−925 nm) in steps of 25 nm. The SEM image of one particular nanorod is visible in Figure 2b. These subwavelength objects were illuminated by the infrared light of a pulsed femtosecond laser.

Panels c and d of Figure 2 report the experimental PEEM images of the 6 × 6 resonator grid acquired at specific excitation wavelength. The PEEM pictures correspond to wide fields of view so as to embrace the whole 6 × 6 resonator matrix and correspond to normal (c) or grazing (d) incidence. Experimentally, a full set of PEEM pictures has been recorded at different wavelengths covering the range (740−880 nm).

For comparison, panels e and f of Figure 2 shows the computed spectral response of the rod resonator grid under normal and grazing incidence, respectively. For each rod length L, the displayed number is the calculated resonance wavelength $\lambda_0^{Res}(m)$ with $R = 16.5$ nm; the spot area is proportional to the resonance intensity and its color indicates the m-resonance order. Experimentally the near field profile, i.e., the charge distribution along the rod longitudinal axis, is proportional to $\partial_x F$. In the current PEEM experiment, the electron emission has its origin in a three-photon absorption process, so the resonance intensity is taken as $\int_{-L/2}^{+L/2}(\partial_x F)^6 dx$. According to the developed model, even and odd m order resonances can be discriminated by an appropriate choice of the incidence angle. Indeed, under normal incidence ($k_{||} = 0$), resonances of even m order (resonances of the second term in eq 4) are systematically extinguished. Optically, even order resonances correspond to symmetric distributions of spatially stationary surface charges and are thus forbidden.

Considering the simplicity of the resonator model used (homogeneous surrounding media, cylindrical rods, no fitting parameters), the agreement between theory and experiment is remarkable. Indeed, the main experimental spectral features are covered by the model. For resonator lengths in the range (50−175 nm) (top line), only three objects (100, 125, 150) nm exhibit strong resonances in the probed wavelength windows. As shown in the next paragraph, high-resolution PEEM images prove that these resonances correspond to the expected lowest-order dipolar mode $m = 1$. The second (200 nm ≤ L ≤ 325 nm) and third (350 nm ≤ L ≤ 475 nm) lines are of particular interest. Experimentally the second line is extinguished under normal incidence but exhibit strong PEEM signal under grazing ones in agreement with systematic extinction of $m = 2n$ mode under normal incidence. The exact opposite is observed for the third line; while excitation under normal incidence leads to significant electron emission, no signal is detected at grazing illumination in agreement with numerical estimates. As expected, the longer the rod lengths, the higher the resonance orders. For example,

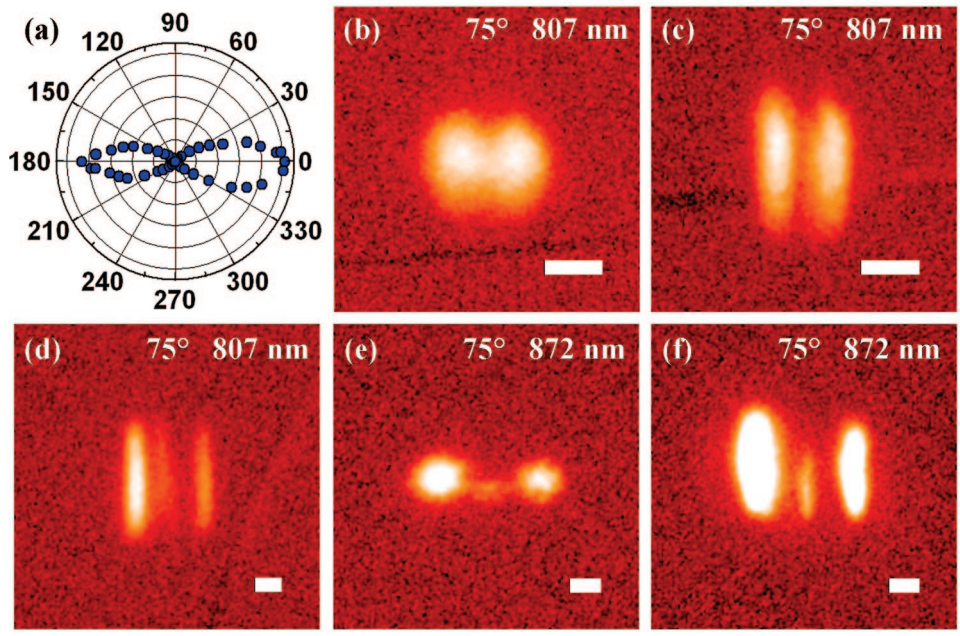

Figure 3. Resonant single Au nanorod investigation. (a) Polar diagram of the photoemission yield vs the polarization angle of a single nanorod (rod length $L = 100$ nm, incident angle $\alpha = 0°$, excitation wavelength $\lambda_0 = 800$ nm, incident power $P = 43$ MW/cm^2). (b) PEEM near-field mapping of a dipolar mode of a resonant nanorod ($L = 100$ nm, $\lambda_0 = 807$ nm, $P = 75$ MW/cm^2). Longitudinal resolution is 41 nm.[19] (c) Same as (b) but with adapted PEEM focus so as to enhance the spatial resolution along the rod axis at the expense of the perpendicular ones. Longitudinal resolution is 25 nm.[19] (d) PEEM near-field mapping of a quadrupolar mode of a resonant nanorod ($L = 250$ nm, $\lambda_0 = 807$ nm, $P = 100$ MW/cm^2), (e) PEEM near field mapping of a quadrupolar mode of a resonant nanorod ($L = 325$ nm, $\lambda_0 = 872$ nm, $P = 55$ MW/cm^2). (f) Same as (e) but with enhanced longitudinal resolution. For all pictures the white scale bar is 100 nm and the color scale is logarithmic. For panels b to f, $\alpha = 75°$, light is p polarized and incident along the rod longitudinal axis.

resonators of length $L = 650$–775 nm (Figure 2f bottom line – 1) show resonances corresponding to $m = 5$.

Single object analysis is one key point of the photoemission electron microscopy. So, spectral investigation and high-resolution near-field mapping have been carried out to ascertain the optical resonant nature of individual rods. Figure 3a shows the polar diagram of the photoemission yield for a single 100 nm rod recorded under normal incidence at 800 nm excitation wavelength. The photoemission yield exhibits the polarization angle dependence expected for a dipolar resonance ($m = 1$) presenting maxima for electrical field parallel to the rod main axis (lightning rod effect[33]). For completeness, direct near-field mapping of this rod has been recorded. The near-field profile, i.e., the charge distribution along the rod longitudinal axis, is proportional to $\partial_x F$. Then as visible in the PEEM imaging (Figure 3b,c), regions of high near-field confinement at both rod ends confirms the dipolar nature of the rod resonance.

Higher order modes can be predicted with the help of eq 5. For instance, in the 225 nm $\leq L \leq$ 300 nm range (second line), rod resonances are predicted to correspond to the $m = 2$ mode (Figure 2f, green spots). The latter $m = 2$ resonance corresponds to a quadrupolar mode with stationary charge localizations at positions (0, $^1/_2$, 1) L. These predictions are readily confirmed by PEEM imaging. Panels d−f of Figure 3 display the near field mappings of the $L = 250$ nm and $L = 325$ nm rod recorded at 807 and 872 nm excitation wavelength, respectively. In both cases a quadrupolar mode is identified around the expected resonance wavelengths.

Higher order modes accessible under grazing incidence are imaged as asymmetric resonances. Formally, under normal incidence a resonance of order m results in a distribution of near-field peaks along the rod axis with the period L/m. Under grazing incidence, the L/m period is roughly preserved; however the predicted field intensity profile becomes asymmetric. As a consequence, resonances of long objects are observed as fragmentary standing wave patterns; i.e., not all confinement regions are simultaneously visible.

In conclusion, short-range surface plasmon polariton resonators have been experimentally investigated at the nanometre scale. To that aim Au nanorods 30 nm in diameter have been microfabricated by electron beam lithography and probed by multiphoton photoemission electron microscopy under free-space laser light excitation. Starting with long nanowire of subwavelength cross section, a SR-SPP transverse magnetic waveguiding mode is evidenced. For rod dimensions shorter than the attenuation length of the propagating SR-SPP wave, standing waves are observed, forming a full set of discrete rod resonances, from the lowest order dipolar ($m = 1$) up to higher-order multipolar modes ($m = 5$). These observations are readily interpreted within the framework of a simple analytical resonator model. With the constant improving of microfabricating techniques in terms of device miniaturization, the present investigation confirms the likely key role to be played by short-range surface plasmon polaritons in photonic devices in the near future.

These advances have been made possible thanks to the high resolution and local-probe-free nature of the multiphoton

PEEM technique. Further improvements will take care of the presence of an interface and the exact geometry of the nanorod cross section.

Acknowledgment. The authors from CEA Saclay thank F. Merlet for expert technical support during PEEM experiment and A. Ghorbal for additional atomic force microscopy studies.

References

(1) Barnes, W. L.; Dereux, A.; Ebbesen, T. W. *Nature* **2003**, *424*, 824–830.
(2) Greffet, J. J. *Science* **2005**, *308*, 1561–1562.
(3) van Hulst, N. F. *Nature* **2007**, *448*, 141–142.
(4) Taminiau, T. H.; Moerland, R. J.; Segerink, F. B.; Kuipers, L.; van Hulst, N. F. *Nano Lett.* **2007**, *7*, 28–33.
(5) Stockman, M. I. *Phys. Rev. Lett.* **2004**, *93*, 137404–137407.
(6) Søndergaard, T.; Bozhevolnyi, S. *Phys. Rev. B* **2007**, *75*, 73402–73405.
(7) Muhlschlegel, P.; Eisler, H. J.; Martin, O. J. F.; Hecht, B.; Pohl, D. W. *Science* **2005**, *308*, 1607–1609.
(8) Cubukcu, E.; Kort, E. A.; Crozier, K. B.; Capasso, F. *Appl. Phys. Lett.* **2006**, *89*, 93120–93122.
(9) Neubrech, F.; Kolb, T.; Lovrincic, R.; Fahsold, G.; Pucci, A.; Aizpurua, J.; Cornelius, T. W.; Toimil-Molares, M. E.; Neumann, R.; Karim, S. *Appl. Phys. Lett.* **2006**, *89*, 253104–253106.
(10) Payne, E. K.; Shuford, K. L.; Park, S.; Schatz, G. C.; Mirkin, C. A. *Journal of Physical Chemistry B* **2006**, *110*, 2150–2154.
(11) Cinchetti, M.; Gloskovskii, A.; Nepjiko, S. A.; Schonhense, G.; Rochholz, H.; Kreiter, M. *Phys. Rev. Lett.* **2005**, *95*, 257403–257406.
(12) Kubo, A.; Onda, K.; Petek, H.; Sun, Z. J.; Jung, Y. S.; Kim, H. K. *Nano Lett.* **2005**, *5*, 1123–1127.
(13) Munzinger, M.; Wiemann, C.; Rohmer, M.; Guo, L.; Aeschlimann, M.; Bauer, M. *New J. Phys.* **2005**, *7*, 68–83.
(14) Douillard, L.; Charra, F.; Fiorini, C.; Adam, P. M.; Bachelot, R.; Kostcheev, S.; Lerondel, G.; de la Chapelle, M. L.; Royer, P. *J. Appl. Phys.* **2007**, *101*, 83518–83522.
(15) Heringdorf, F. M. Z.; Chelaru, L. I.; Mollenbeck, S.; Thien, D.; Hoegen, M. H. V. *Surf. Sci.* **2007**, *601*, 4700–4705.
(16) Kubo, A.; Pontius, N.; Petek, H. *Nano Lett.* **2007**, *7*, 470–475.
(17) Dickson, R. M.; Lyon, L. A. *J. Phys. Chem. B* **2000**, *104*, 6095–6098.
(18) Sönnichsen, C.; Franzl, T.; Wilk, T.; von Plessen, G.; Feldmann, J.; Wilson, O.; Mulvaney, P. *Phys. Rev. Lett.* **2002**, *88*, 077402-077405.
(19) Huang, H. J.; Yu, C. P.; Chang, H. C.; Chiu, K. P.; Chen, H. M.; Liu, R. S.; Tsai, D. P. *Opt. Express* **2007**, *15*, 7132–7139.
(20) Seong Keun, K.; Okamoto, H.; Jong Kuk, L.; Imura, K.; Nagahara, T. *Chem. Phys. Lett.* **2005**, *412*, 41–45.
(21) Ditlbacher, H.; Hohenau, A.; Wagner, D.; Kreibig, U.; Rogers, M.; Hofer, F.; Aussenegg, F. R.; Krenn, J. R. *Phys. Rev. Lett.* **2005**, *95*, 257403–257406.
(22) The lateral resolution is defined by the horizontal distance over which the intensity drops from 84% to 16% of maximum signal.
(23) The current LEEM/PEEM instrument works in total electron yield which increases its sensitivity at the price of a loss of spatial resolution originating from the energy spread of the electrons contributing to the image formation (chromatic aberration).
(24) Wiederrecht, G. P. *Eur. Phys. J.: Appl. Phys.* **2004**, *28*, 3–18.
(25) Nelayah, J.; Kociak, M.; Stephan, O.; de Abajo, F. J. G.; Tence, M.; Henrard, L.; Taverna, D.; Pastoriza-Santos, I.; Liz-Marzan, L. M.; Colliex, C. *Nat. Phys.* **2007**, *3*, 348–353.
(26) Vesseur, E. J. R.; Waele, R. d.; Kuttge, M.; Polman, A. *Nano Lett.* **2007**, *7*, 2843–2846.
(27) Salomon, L.; Bassou, G.; Aourag, H.; Dufour, J. P.; de Fornel, F.; Carcenac, F.; Zayats, A. V. *Phys. Rev. B* **2002**, *65*, 125409–125413.
(28) Novotny, L. *Phys. Rev. Lett.* **2007**, *98*, 266802–266805.
(29) Coefficients values are computed from $a_1 = 13.74 - 0.12(\varepsilon_\infty + 141.04\varepsilon_s)/\varepsilon_s$ and $a_2 = 0.12\sqrt{\varepsilon_\infty + 141.04\varepsilon_s}/\varepsilon_s$. More details can be found in ref 28.
(30) Raether, H. *Springer Tracts Mod. Phys.* **1988**, 111.
(31) Klyuchnik, A. V.; Kurganov, S. Y.; Lozovik, Y. E. *Phys. Solid State* **2003**, *45*, 1327–1331.
(32) Lamprecht, B.; Schider, G.; Lechner, R. T.; Ditlbacher, H.; Krenn, J. R.; Leitner, A.; Aussenegg, F. R. *Phys. Rev. Lett.* **2000**, *84*, 4721–4724.
(33) Van Bladel, J. G. *Singular Electromagnetic Fields and Sources*; Wiley IEEE Press: New York, 1996; ISBN 978-0-7803-6038-9.

NL080053V